

Observation of power amplification in a self-injecting laser wakefield accelerator

M.J.V. Streeter^{1,2,3,*}, S. Kneip³, M.S. Bloom³, R.A. Bendoyro⁴, O. Chekhlov⁵, A.E. Dangor³,
A. Döpp³, C.J. Hooker⁵, J. Holloway⁶, J. Jiang⁴, N.C. Lopes^{3,4}, H. Nakamura³, P.A. Norreys⁵,
C.A.J. Palmer^{1,2}, P.P. Rajeev⁵, J. Schreiber^{7,8}, D.R. Symes⁵, M. Wing⁶, S.P.D. Mangles³, and Z. Najmudin³

¹ *The Cockcroft Institute, Keckwick Lane, Daresbury, WA4 4AD, United Kingdom*

² *Physics Department, Lancaster University, Lancaster LA1 4YB, United Kingdom*

³ *John Adams Institute for Accelerator Science, The Blackett Laboratory,*

Imperial College London, London, SW7 2AZ, United Kingdom

⁴ *GoLP/Instituto de Plasmas e Fusão Nuclear, Instituto Superior Técnico,*

Universidade de Lisboa, Lisboa 1049-001, Portugal

⁵ *Central Laser Facility, Rutherford Appleton Laboratory, Chilton, Oxon, OX11 0QX, United Kingdom*

⁶ *Department of Physics and Astronomy, University College London, London WC1E 6BT, United Kingdom*

⁷ *Fakultät für Physik, Ludwig-Maximilians-Universität München,*

Coulombwall 1, D-85748 Garching, Germany and

⁸ *Max-Planck-Institut für Quantenoptik, Hans-Kopfermann-Str. 1, D-85748 Garching, Germany*

(Dated: October 18, 2017)

We report on the depletion and power amplification of the driving laser pulse in a strongly-driven laser wakefield accelerator. Simultaneous measurement of the transmitted pulse energy and temporal shape indicate an increase in peak power from 187 ± 11 TW to a maximum of 318 ± 12 TW after 13 mm of propagation in plasma density of $0.9 \times 10^{18} \text{ cm}^{-3}$. The power amplification is correlated with the injection and acceleration of electrons in the non-linear wakefield. This process is modeled by including localized redshifting and subsequent group delay dispersion at the laser pulse front.

PACS numbers: 41.75.Jv, 42.65.Jx, 52.38.Dx, 52.38.Hb, 52.38.Kd, 52.65.Rr

Laser wakefield accelerators (LWFA) [1] can now produce electron beams with particle energies greater than GeV from an interaction length of just a few centimeters [2–4]. In these devices, a high-intensity laser pulse, propagating through a plasma, initiates a wavelike electron density perturbation. This wakefield exhibits extremely high longitudinal electric fields that can serve to accelerate charged particles.

Numerous methods have been demonstrated to inject particles within a LWFA [5]. Of these, self-injection in the highly non-linear [6–8], sometimes called ‘bubble’, regime is amongst the simplest and thus most common [2]. By using self [9] or external guiding [10], it is possible to maintain the laser wakefield accelerator far beyond the normal Rayleigh diffraction length. However, the eventual energy gain of electrons by the wakefield is limited either by *dephasing*, or by energy *depletion* of the driving laser pulse [11].

Dephasing occurs when electrons gain sufficient energy to outrun the wakefield, which is usually said to move at the linear group velocity of the laser pulse in the plasma, $v_g = c\sqrt{1 - \omega_p^2/\omega_0^2}$, where ω_p and ω_0 are the plasma and laser angular frequencies respectively. For a linear relativistic plasma wave, (i.e. with wavelength $\lambda_p = 2\pi c/\omega_p$ and Lorentz factor $\gamma_\phi \approx \sqrt{n_c/n_e} \gg 1$), the dephasing length is $L_d = \gamma_\phi^2 \lambda_p = (\omega_0/\omega_p)^2 \lambda_p$, where $n_c = \epsilon_0 m_e \omega_0^2 / e^2$ is the critical density. The dephasing length, hence, increases with decreasing plasma density, n_e .

The length over which the laser energy is depleted, L_{dp} , is determined by the plasma wave generation pro-

cess. For a short duration laser pulse driving a non-linear wakefield, (pulse length $\sigma_t < \lambda_p/c$ and normalized vector potential $a_0 \gg 1$), plasma electrons are pushed outward by the front of the pulse such that the rear of pulse propagates in an ion cavity. Pump depletion occurs at the front of the laser pulse as energy is coupled into the plasma wave or lost due to diffraction. As a result of this localized depletion, the driving laser rapidly evolves to have a sharp rising edge, which etches back through the pulse [12, 13].

Decker *et al.* [12] showed that the velocity of this pulse front etching is $v_{\text{etch}} = c\omega_p^2/\omega_0^2$ in the group velocity frame of the laser. The depletion length is then

$$L_{dp} \approx (\omega_0^2/\omega_p^2)\sigma_t c. \quad (1)$$

For a near-resonant pulse, $c\sigma_t \approx \lambda_p$, then $L_{dp} \approx L_d$, and so depletion should not affect energy gain. However, because of pulse front erosion, the effective laser pulse velocity is reduced, such that the plasma wave phase velocity becomes $v_\phi = v_g - v_{\text{etch}} \approx c[1 - \frac{3}{2}(\omega_p^2/\omega_0^2)]$ for $\omega_p \ll \omega_0$. This reduces the dephasing length to $L_d = 2/3(\omega_0/\omega_p)^2 \lambda_p$, and limits the maximum energy gain produced by the wakefield [11].

The pulse front etching model, which considers complete energy depletion of the front of the laser pulse at a constant rate, does not describe power amplification of the pulse. However, simulations suggest that the laser power will increase in this regime [14], which is vital for self-injection of electrons [15–17]. Furthermore, the fact that injection is not immediate, but requires some evolution length over which the intensity increases before

injection, means that depletion can severely curtail the acceleration length at low densities [18]. Though pulse front etching has been verified in simulations [11], and guiding has been demonstrated up to L_{dp} for a range of plasma densities [19], no quantitative measurement of pump depletion in non-linear LWFA has been reported. Furthermore, though pulse shortening of LWFA drivers has been reported [20, 21], there are, as yet, no direct experimental measurements of an increase in peak laser power.

In this letter, we present measurements of laser energy depletion and pulse compression of a relativistic ($a_0 \gg 1$) short-pulse ($c\sigma_t < \lambda_p$) laser in a self-guided LWFA. We find that depletion is well described by pulse front erosion, but we also observe, for the first time, direct measurement of power amplification of the driving laser pulse. The power amplification can be understood by modifying the pulse front etching model so that photons at the pulse front are downshifted in energy until they are traveling at the plasma wave phase velocity. The power amplification was found to be coincident with the onset of electron self-injection, confirming its vital role in this process.

The experiment was performed using the Astra Gemini laser [22] at the Rutherford Appleton Laboratory, interacting with a supersonic helium gas jet. A 15 mm diameter nozzle was used, which gave an interaction length of 13.0 mm at electron densities of up to $n_e = 4 \times 10^{18} \text{ cm}^{-3}$, or $0.007 n_c$. Each linear polarized laser pulse, of wavelength $\lambda_0 = 800 \text{ nm}$, contained $11 \pm 1 \text{ J}$ of energy in a duration of $t_{FWHM} = 51 \pm 3 \text{ fs}$. The laser was focused onto the front of the gas target with an $f/20$ parabolic mirror at a peak $a_0 \simeq 3.0$.

A magnetic electron spectrometer was used to measure the spectrum of the accelerated electron beam. The fluence of the laser pulse at the exit plane of the plasma was imaged with a pair of $f/10$ spherical mirrors at a resolution of $10 \mu\text{m}$ over a field of view of $902 \mu\text{m} \times 675 \mu\text{m}$. The transmitted energy was measured by integrating the counts on the camera, which was cross-calibrated with an energy diode. Also, a 5 mm diameter area near the center of the transmitted beam, $\approx 1/20^{\text{th}}$ of the full beam diameter, was directed to two Grenouille (Swamp Optics) SHG-FROGs (second harmonic generation - frequency resolved optical gating) [23]. These devices produced spectrally dispersed auto-correlations, from which the complete temporal intensity and phase information of the pulse was retrieved using an iterative algorithm.

The first FROG could measure to a lower pulse length limit of 10 fs, for a time-bandwidth limited pulse, while the second was restricted to 20 fs due to the limited phase matching bandwidth of its second harmonic crystal. For shots where both FROGs could be used, the second was used to determine the time direction of the first. This was achieved by placing additional glass in the beam path of the second FROG to create a known spectral phase offset

between the two. Only retrieved pulses with the correct time direction have the correct phase offset, and so incorrect retrievals can be eliminated. This process was only possible for $n_e < 0.6 \times 10^{18} \text{ cm}^{-3}$. At higher density, the spectrum became too broad for the second FROG. For these measurements, gradual changes of the pulse shape and Wigner [24] transforms with increasing density were used to determine the direction of time. The phase retrieval algorithm was performed 10 times, each time with a different random seed, for each shot to provide an indication of the robustness of the retrieval process. The pulse variations were included in the calculation of measurement error. Shots with visibly poor retrievals, large FROG errors (RMS relative pixel error > 0.02) or large time direction uncertainties were not included in the results. Out of 59 shots, 43 have been included.

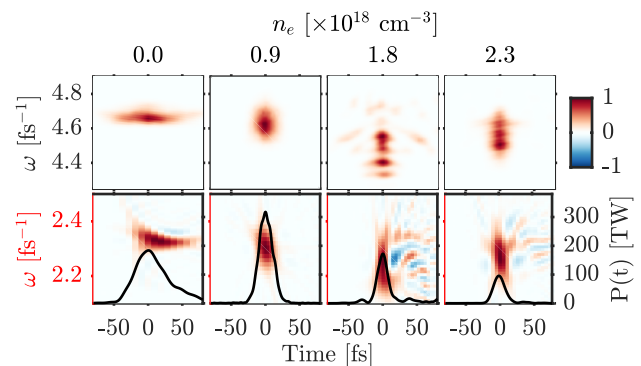


Figure 1. (Top) Raw FROG traces and (bottom) Wigner transforms with temporal profiles (black lines) for (left-to-right) $n_e = (0, 0.9, 1.8, 2.3) \times 10^{18} \text{ cm}^{-3}$. The Wigner transforms and temporal profiles have been corrected for dispersion in the beamline and represent the pulse at the plasma exit.

Examples of the measured FROG traces and retrieved pulses are shown in fig. 1. The pulse was observed to frequency downshift and temporally compress for increasing plasma density up to $n_e = 1.5 \times 10^{18} \text{ cm}^{-3}$. Beyond this, the pulse length increased again due to energy depletion of the laser pulse.

The results are shown as a function of plasma density in fig. 2. For the plots of pulse energy transmission (fig. 2a), transmitted pulse length (fig. 2b) and peak power (fig. 2c), each data point represents one measurement. The maximum accelerated electron energy (fig. 2c) values were averaged over multiple (~ 4) shots within a density bin width of $0.2 \times 10^{18} \text{ cm}^{-3}$. The error in the measured maximum electron energy was estimated from the blurring effect of the measured electron beam divergence on the spectrometer screens. This was combined in quadrature with the standard error. The ratio of the interaction length to L_{dp} (eq. (1)) is shown for comparison at the top of fig. 2a, with $\sigma_t = t_{FWHM}/\sqrt{2 \ln(2)}$.

Laser energy depletion was seen to increase with increasing density (fig. 2a). About 50% of the energy was

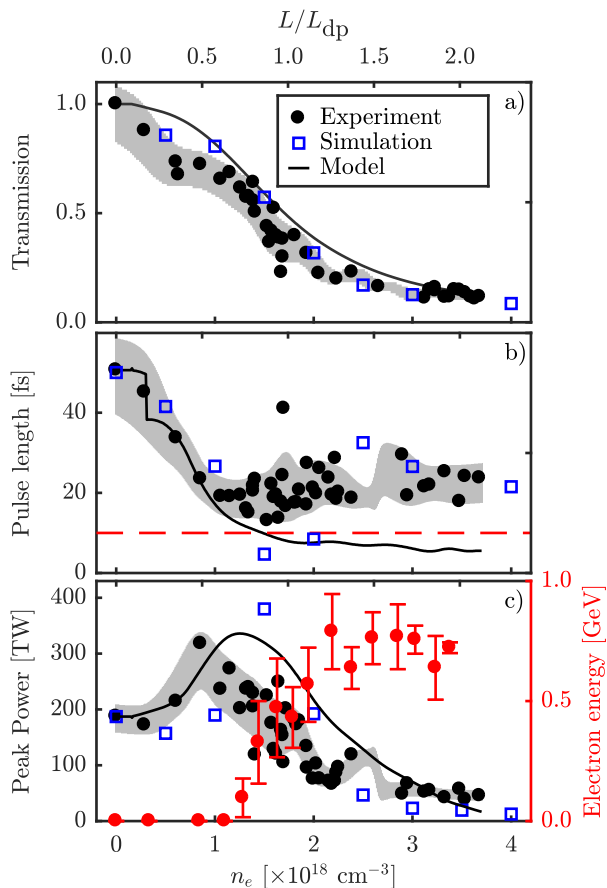


Figure 2. Experimental and simulated: **a)** transmitted laser energy fraction, **b)** pulse duration (FWHM) and **c)** peak pulse power and maximum observed electron beam energy (red circles), against plasma density. The solid black lines are calculations made with the new pulse depletion and compression model. The grey shaded regions indicate RMS error (statistical and measurement errors) of a moving average of the data points. The measurement errors are used for the quoted pulse values in this paper. The red dashed line in **b)** is the instrument limit of the FROG for time-bandwidth limited pulses.

transmitted for $L = L_{dp}$, whilst the beam was almost fully depleted for $L = 2L_{dp}$. Imaging of the exit plane showed a guided spot for $n_e > 1 \times 10^{18} \text{ cm}^{-3}$, while for $n_e > 3 \times 10^{18} \text{ cm}^{-3}$, only the unguided fraction of the laser energy was observed, corresponding to $\approx 15\%$ of the input laser energy. The measured pulse duration (fig. 2b) decreased from an initial 51 ± 3 fs to the shortest observed pulse length of 13.0 ± 1.3 fs for $n_e = 1.5 \times 10^{18} \text{ cm}^{-3}$. The peak power of the laser pulse after the interaction (fig. 2c) was calculated by setting the energy of the transmitted pulse equal to the time integral of the temporal pulse shape. As a result of the pulse compression, the power was observed to increase, with a maximum at $n_e = 0.9 \times 10^{18} \text{ cm}^{-3}$, increasing from 187 ± 11 TW to 318 ± 12 TW. At this density, the pulse length was shortened to 23.4 ± 1.2 fs FWHM, while the transmission was

still $72 \pm 8\%$. At higher densities, additional pump depletion means that even though the pulse was compressed further, the peak power dropped.

Wide-angle electron emission was produced for $n_e > 0.2 \times 10^{18} \text{ cm}^{-3}$ but the charge increased significantly for $n_e > 1.1 \times 10^{18} \text{ cm}^{-3}$ (fig. 2c.), where the maximum power enhancement was observed. The maximum beam energies, of 0.79 ± 0.14 GeV, occurred at $n_e \approx 2.3 \times 10^{18} \text{ cm}^{-3}$.

The experiment was simulated using the OSIRIS [25] particle-in-cell code in a 2D3V geometry. The simulation window moved at c along the laser propagation direction and had dimensions of $200 \mu\text{m} \times 200 \mu\text{m}$ divided into 8000×8000 cells in the pulse propagation (z) and the transverse (x) directions respectively. The pulse envelope was modeled using a polynomial approximation to a Gaussian with a FWHM duration of 50 fs, focused to a spot width FWHM of $25 \mu\text{m}$ and a peak a_0 of 3.0. The plasma target was 15 mm in length, including linear density ramps over $500 \mu\text{m}$ at the entrance and exit of the plasma, with 4 electron macro-particles per cell and stationary ions.

The simulated pulse properties at the plasma exit are shown alongside the experimental data in fig. 2. The energy depletion and pulse compression rates proceeded at similar rates to the experimental data, but the pulse compressed to a lower minimum of 4 fs at $n_e = 1.5 \times 10^{18} \text{ cm}^{-3}$. At higher densities, the pulse length increased again, once almost all the laser energy was depleted and the compressed peak in the laser field dissipated.

Figure 3a shows the propagation dependence of the on-axis plasma density modulation in the reduced group velocity ($v_\phi = v_g - v_{\text{etch}}$) reference frame, for a density of $n_e = 4 \times 10^{18} \text{ cm}^{-3}$. The laser peak a_0 , plotted as a red line, first increased via pulse compression, and then decreased due to pump depletion. Self-focusing was observed in the first 1 mm of plasma, after which a stable guided spot size was reached. Close agreement was seen with the pulse front etching model [12], as the density peak, coinciding with the leading edge of the laser pulse, moved at close to the reduced group velocity. Deviation from this velocity was seen at early times, before the sharp front of the driving pulse was formed, and at late times, once the laser was mostly depleted.

Rapid compression of the driving pulse occurs 4 mm into the target and causes the radius of the plasma bubble, r_b , to increase, since $r_b \propto \sqrt{a_0}$ [26]. During this stage of the interaction, the effective phase velocity of the back of the wake decreases from $\gamma_\phi = 20$ to $\gamma_\phi = 7$. This coincided with self-injection of plasma electrons [27], as seen by the straight lines of high density originating from the back of the first plasma wave period and advancing relative to the plasma wave as the simulation progresses. The injection occurred over a short propagation distance, populating a narrow phase region of the wakefield, similar

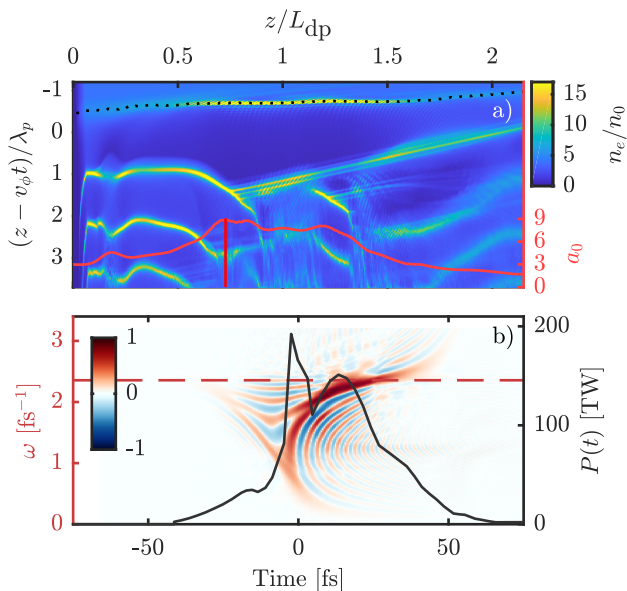


Figure 3. **a)** On-axis electron density map (image) in a frame moving at $v_\phi = v_g - v_{\text{etch}}$ and peak a_0 of the laser (red line) as a function of propagation distance in a simulation for plateau electron density $n_0 = 4 \times 10^{18} \text{ cm}^{-3}$. The first maxima of the plasma wave, which coincides with the leading edge of the laser pulse, is overlaid with a black dashed line. **b)** Wigner transform (blue-red) of the laser pulse overlaid with the temporal intensity profile at $z = 0.7L_{dp}$ (3.9 mm). The red horizontal line shows the initial frequency of the laser.

to injection mechanisms that use tailoring of the target density profile to modify the plasma wave phase velocity [15, 28, 29].

The pulse frequency shift and compression is illustrated by the Wigner transform of the simulated laser pulse at $z = 4 \text{ mm}$ in fig. 3b. The pulse was largely redshifted at the first density maximum of the plasma wave, close to the maximum of the laser intensity, as discussed in [21]. The increase in spectral bandwidth allowed the pulse length to shorten.

Assuming that all the laser energy ahead of the density spike is downshifted to zero frequency, and so fully depleted, gives an etching rate consistent with eq. (1). However, this precludes the possibility of increasing the laser energy behind the depletion region, which occurs due to group velocity dispersion. Downshifted photons will slip back through the pulse away from the depletion region before losing all their energy, as seen in fig. 3b. Equating the group velocity of a redshifted photon to the reduced group velocity of the laser pulse front, $v_g(\omega_{\text{min}}) = v_g(\omega_0) - v_{\text{etch}}$, gives the minimum frequency reached by these photons as $\omega_{\text{min}} = \omega_0 / \sqrt{3}$. Assuming that the pulse front moves back once the local power drops below the critical power for self-focusing P_c , then the energy depleted from a local region in the power profile $P(t)\Delta t$ is limited to $(1 - 1/\sqrt{3})(P(t) - P_c)\Delta t$. The

remainder, $(P(t) - P_c)\Delta t / \sqrt{3}$, moves back through the pulse, towards the ion cavity where the group velocity dispersion is much smaller. This leads to an increase in power behind the depletion front, and thereby modifies the energy depletion rate.

Numerical calculations were performed, by stepping through the measured initial power profile $P(t)$ from the first point at which $P(t) > P_c$ for a given plasma density, reducing the power at this point to $P(t) = P_c$. The un-depleted fraction of this energy, $(P(t) - P_c)\Delta t / \sqrt{3}$, is added to the following region of the pulse, averaged over $\lambda_p/4$ to approximate the effect of group velocity dispersion. The pulse energy, duration and peak power after propagating 13 mm were calculated at each density and are plotted as black lines in fig. 2.

The numerical model is seen to accurately predict the energy depletion rate observed experimentally. The pulse compression results are well reproduced, until $n_e > 1 \times 10^{18} \text{ cm}^{-3}$, where the pulse length reaches a lower value than can be measured experimentally. The sudden drop in pulse length at $n_e \approx 0.3 \times 10^{18} \text{ cm}^{-3}$ occurs at the threshold where the peak power exceeds $2P_c$, such that the regions of the pulse etched to P_c no longer contributed to the FWHM pulse length value. The power amplification effect is well matched for low densities, with the model predicting that the maximum power will be reached for $n_e = 1.3 \times 10^{18} \text{ cm}^{-3}$. Experimental power measurements at this density are likely to be an underestimate, as the pulse spectrum was broader than the phase matching bandwidth in the FROG diagnostic.

For a Gaussian laser pulse with the initial peak power $P_0 > P_c$, maximum power amplification is reached when the pulse is etched to approximately the midway point, and the laser pulse energy is reduced by $\sim 50\%$. This occurs after a propagation distance

$$L_{\text{evol}} = \sigma_t c \left(\frac{2\omega_0^2}{3\omega_p^2} \right) \sqrt{\frac{1}{2} \ln \left(\frac{P_0}{P_c} \right)}, \quad (2)$$

For moderate values of P_0/P_c , ($n_e > 0.6 \times 10^{18} \text{ cm}^{-3}$ in fig. 2), the evolution length is approximately equal to the usually quoted depletion length L_{dp} , and the pulse is only fully depleted at $L \approx 2L_{\text{evol}}$. Taking the injection point to occur at this evolution distance ($z_{\text{inj}} = L_{\text{evol}}$), pump depletion of a 180 TW 50 fs pulse occurs before dephasing for $n_e < 4.2 \times 10^{18} \text{ cm}^{-3}$. At the density for which the maximum electron energy was observed in the experiment, $n_e = 2.3 \times 10^{18} \text{ cm}^{-3}$, injection occurs at $z = 8.6 \text{ mm}$ into the plasma, giving an acceleration length of 4.4 mm. However, the initial pulse shape in the experiment was non-Gaussian, having a rapid rising edge and an extended falling edge. As a result of this, L_{evol} was shortened to 7.2 mm, with the consequence that more laser energy remained in the pulse, allowing the acceleration length to be extended to 5.8 mm. Using this value, and the experimentally measured electron energy, the av-

erage acceleration gradient over this acceleration length was $\approx 140 \text{ GeVm}^{-1}$.

This modified pulse evolution model enables optimisation of electron beams produced by self-injecting laser wakefield accelerators through tailoring of the laser pulse shape. The energy lost before injection can be minimized by using a sharp rising edge to the laser pulse. A slow falling edge then allows a large a_0 to be maintained over an extended acceleration length. In this way, electron beam energy can be maximized, benefiting the many applications of these accelerators, such as in the generation of large numbers of x-rays [30], gamma rays [31] and positrons [32].

We would like to acknowledge technical support from CLF staff. This research was supported by STFC (ST/J002062/1, ST/P000835/1), and EPSRC (EP/I014462/1). We thank the OSIRIS consortium (UCLA/IST) for the use of OSIRIS. M. Wing acknowledges the support of DESY, Hamburg and the Alexander von Humboldt Stiftung.

* matthew.streeter@cockcroft.ac.uk

-
- [1] T. Tajima and J. M. Dawson, *Physical Review Letters* **43**, 267 (1979).
- [2] W. P. Leemans, A. J. Gonsalves, H.-S. Mao, K. Nakamura, C. Benedetti, C. B. Schroeder, C. Tóth, J. Daniels, D. E. Mittelberger, S. S. Bulanov, J.-L. Vay, C. G. R. Geddes, and E. Esarey, *Physical Review Letters* **113**, 245002 (2014).
- [3] X. Wang, R. Zgadaj, N. Fazel, Z. Li, S. A. Yi, X. Zhang, W. Henderson, Y.-Y. Chang, R. Korzekwa, H.-E. Tsai, C.-H. Pai, H. Quevedo, G. Dyer, E. Gaul, M. Martinez, A. C. Bernstein, T. Borger, M. Spinks, M. Donovan, V. Khudik, G. Shvets, T. Ditmire, and M. C. Downer, *Nature Communications* **4**, 1988 (2013).
- [4] H. T. Kim, K. H. Pae, H. J. Cha, I. J. Kim, T. J. Yu, J. H. Sung, S. K. Lee, T. M. Jeong, and J. Lee, *Physical Review Letters* **111**, 165002 (2013).
- [5] E. Esarey, C. Schroeder, and W. Leemans, *Reviews of Modern Physics* **81**, 1229 (2009).
- [6] S. P. D. Mangles, C. D. Murphy, Z. Najmudin, A. G. R. Thomas, J. L. Collier, A. E. Dangor, E. J. Divall, P. S. Foster, J. G. Gallacher, C. J. Hooker, D. A. Jaroszynski, A. J. Langley, W. B. Mori, P. A. Norreys, F. S. Tsung, R. Viskup, B. R. Walton, and K. Krushelnick, *Nature* **431**, 535 (2004).
- [7] C. G. R. Geddes, C. S. Toth, J. Van Tilborg, E. Esarey, C. B. Schroeder, D. Bruhwiler, C. Nieter, J. Cary, and W. P. Leemans, *Nature* **431**, 538 (2004).
- [8] J. Faure, Y. Glinec, A. Pukhov, S. Kiselev, S. Gordienko, E. Lefebvre, J.-P. Rousseau, F. Burgy, and V. Malka, *Nature* **431**, 541 (2004).
- [9] A. G. R. Thomas, Z. Najmudin, S. P. D. Mangles, C. D. Murphy, A. E. Dangor, C. Kamperidis, K. L. Lancaster, W. B. Mori, P. A. Norreys, W. Rozmus, and K. Krushelnick, *Physical Review Letters* **98**, 095004 (2007).
- [10] D. J. Spence and S. M. Hooker, *Physical Review E - Statistical, Nonlinear, and Soft Matter Physics* **63**, 1 (2001).
- [11] W. Lu, M. Tzoufras, C. Joshi, F. Tsung, W. Mori, J. Vieira, R. Fonseca, and L. Silva, *Physical Review Special Topics - Accelerators and Beams* **10**, 061301 (2007).
- [12] C. D. Decker, W. B. Mori, K.-C. Tzeng, and T. Katsouleas, *Physics of Plasmas* **3**, 2047 (1996).
- [13] J. Vieira, F. Fiúza, L. O. Silva, M. Tzoufras, and W. B. Mori, *New Journal of Physics* **12** (2010).
- [14] D. F. Gordon, B. Hafizi, R. F. Hubbard, J. R. Peñano, P. Sprangle, and A. Ting, *Physical Review Letters* **90**, 215001 (2003).
- [15] S. Kalmykov, S. A. Yi, V. Khudik, and G. Shvets, *Physical Review Letters* **103**, 135004 (2009).
- [16] S. Kneip, S. R. Nagel, S. F. Martins, S. P. D. Mangles, C. Bellei, O. Chekhlov, R. J. Clarke, N. Delerue, E. J. Divall, G. Doucas, K. Ertel, F. Fiúza, R. Fonseca, P. Foster, S. J. Hawkes, C. J. Hooker, K. Krushelnick, W. B. Mori, C. A. J. Palmer, K. Ta Phuoc, P. P. Rajeev, J. Schreiber, M. J. V. Streeter, D. Urner, J. Vieira, L. O. Silva, and Z. Najmudin, *Physical Review Letters* **103**, 035002 (2009).
- [17] A. Sävert, S. P. D. Mangles, M. Schnell, E. Siminos, J. M. Cole, M. Leier, M. Reuter, M. B. Schwab, M. Möller, K. Poder, O. Jäckel, G. G. Paulus, C. Spielmann, S. Skupin, Z. Najmudin, and M. C. Kaluza, *Physical Review Letters* **115**, 055002 (2015).
- [18] M. S. Bloom, M. J. V. Streeter, S. Kneip, R. A. Bendroyro, O. Cheklov, J. M. Cole, A. Doepp, C. J. Hooker, J. Holloway, J. Jiang, N. C. Lopes, H. Nakamura, P. A. Norreys, P. P. Rajeev, D. R. Symes, J. Schreiber, J. C. Wood, M. Wing, Z. Najmudin, and S. P. D. Mangles, (2017), arXiv:1710.05740.
- [19] J. E. Ralph, K. A. Marsh, A. E. Pak, W. Lu, C. E. Clayton, F. Fang, W. B. Mori, and C. Joshi, *Physical Review Letters* **102**, 175003 (2009).
- [20] J. Faure, Y. Glinec, J. J. Santos, F. Ewald, J.-P. Rousseau, S. Kiselev, A. Pukhov, T. Hosokai, and V. Malka, *Physical Review Letters* **95**, 205003 (2005).
- [21] J. Schreiber, C. Bellei, S. P. D. Mangles, C. Kamperidis, S. Kneip, S. R. Nagel, C. A. J. Palmer, P. P. Rajeev, M. J. V. Streeter, and Z. Najmudin, *Physical Review Letters* **105**, 235003 (2010).
- [22] C. J. Hooker, J. L. Collier, O. Chekhlov, R. Clarke, E. Divall, K. Ertel, B. Fell, P. Foster, S. Hancock, A. Langley, D. Neely, J. Smith, and B. Wyborn, *J. Phys. IV France* **133**, 673 (2006).
- [23] R. Trebino, *Frequency-Resolved Optical Gating: The Measurement of Ultrashort Laser Pulses* (Springer US, Boston, MA, 2000).
- [24] E. Wigner, *Physical Review* **40**, 749 (1932).
- [25] R. A. Fonseca, L. O. Silva, F. S. Tsung, V. K. Decyk, W. Lu, C. Ren, W. B. Mori, S. Deng, S. Lee, T. Katsouleas, and J. C. Adam, in *Computational Science ICCS 2002 SE - 36*, Lecture Notes in Computer Science, Vol. 2331, edited by P. Sloot, A. Hoekstra, C. Tan, and J. Dongarra (Springer Berlin Heidelberg, 2002) pp. 342–351.
- [26] W. Lu, C. Huang, M. Zhou, W. B. Mori, and T. Katsouleas, *Physical Review Letters* **96**, 165002 (2006).
- [27] C. B. Schroeder, C. Benedetti, E. Esarey, and W. P. Leemans, *Physical Review Letters* **106**, 135002 (2011).
- [28] S. Bulanov, N. Naumova, F. Pegoraro, and J. Sakai, *Physical Review E* **58**, R5257 (1998).
- [29] C. G. R. Geddes, K. Nakamura, G. R. Plateau, C. Toth,

- E. Cormier-Michel, E. Esarey, C. B. Schroeder, J. R. Cary, and W. P. Leemans, *Physical Review Letters* **100**, 215004 (2008).
- [30] S. Kneip, C. McGuffey, J. L. Martins, S. F. Martins, C. Bellei, V. Chvykov, F. Dollar, R. Fonseca, C. Huntington, G. Kalintchenko, A. Maksimchuk, S. P. D. Mangles, T. Matsuoka, S. R. Nagel, C. A. J. Palmer, J. Schreiber, K. T. Phuoc, A. G. R. Thomas, V. Yanovsky, L. O. Silva, K. Krushelnick, and Z. Najmudin, *Nature Physics* **7**, 737 (2011).
- [31] G. Sarri, K. Poder, J. M. Cole, W. Schumaker, A. Di Piazza, B. Reville, T. Dzelzainis, D. Doria, L. A. Gizzi, G. Grittani, S. Kar, C. H. Keitel, K. Krushelnick, S. Kuschel, S. P. D. Mangles, Z. Najmudin, N. Shukla, L. O. Silva, D. Symes, A. G. R. Thomas, M. Vargas, J. Vieira, and M. Zepf, *Nature Communications* **6**, 6747 (2015), arXiv:1312.0211.
- [32] G. Sarri, D. J. Corvan, W. Schumaker, J. M. Cole, A. Di Piazza, H. Ahmed, C. Harvey, C. H. Keitel, K. Krushelnick, S. P. D. Mangles, Z. Najmudin, D. Symes, A. G. R. Thomas, M. Yeung, Z. Zhao, and M. Zepf, *Physical Review Letters* **113**, 224801 (2014).